

# Strong polarization-induced reduction of addition energies in single-molecule nanojunctions

Kristen Kaasbjerg and Karsten Flensberg

*Nano-Science Center, Niels Bohr Institute, University of Copenhagen, DK-2100 Copenhagen, Denmark*

We address polarization-induced renormalization of molecular levels in solid-state based single-molecule transistors and focus on an organic conjugate molecule where a surprisingly large reduction of the addition energy has been observed. We have developed a scheme that combines a self-consistent solution of a quantum chemical calculation with a realistic description of the screening environment. Our results indeed show a large reduction, and we explain this to be a consequence of both (a) a reduction of the electrostatic molecular charging energy and (b) polarization induced level shifts of the HOMO and LUMO levels. Finally, we calculate the charge stability diagram and explain at a qualitative level general features observed experimentally.

The recent experimental progress in single-molecule electronics has resulted in the realization of the three-terminal molecular single-electron transistor (SET)<sup>1,2,3,4,5,6,7,8,9,10</sup> shown schematically in Figure 1a. The experimental realizations have been based on a variety of techniques including junctions made by electromigration, mechanical break junctions and cryogenic nanogap fabrication. Many indications of the molecule being part of the active transport pathway through the junction has been observed. An example is the observation of the molecular vibrational excitations, which serve as a fingerprint for the molecule<sup>5</sup>. There remain, however, several unresolved issues in single-molecule transport both in the strong coupling limit, where coherent transport theories seems to strongly overestimate the current level, as well as in the weak coupling regime, where the observed energy gaps are much smaller than expected. Experiments on organic molecules have shown that the so-called addition energy, which is the difference between the molecular ionization potential (IP) and the electron affinity (EA), is heavily reduced compared to its gas phase value in single-molecule SETs<sup>3,5,8</sup>.

Reductions of the excitation gaps is well-known from other situations. Theoretical studies of semiconduc-

tor/metal interfaces have shown that the band-gap of the semiconductor is narrowed near the interface by the screening in the metal<sup>11,12</sup>. Experiments using photoemission techniques and scanning tunneling spectroscopy to study the electronic structure of single molecules, self-assembled monolayers and organic thin films on dielectric and metal surfaces have shown similar effects<sup>13,14,15,16,17,18</sup>. The experimental settings of a single-molecule SET is to some degree analogous to the situation in electrochemical measurements where the equivalent of the addition energy, the electrochemical gap, is well-known to depend on the dielectric properties of the surrounding media<sup>19</sup>. However, the screening environments are rather different for the electrochemical setup and the single-molecule transistor geometry, with one being in ionic solutions or organic solvents and the other in solid state low temperature environment. A direct comparison is therefore not possible in general.

It has been suggested that the reduction of the addition energy seen in single-molecule SETs is caused by polarization/image charges in the metallic electrodes<sup>3,20</sup>, giving rise to a localization of the charges near the metallic electrodes. Theoretically only a few other studies have addressed the polarization induced renormalization of the molecular levels in solid state environments and its implications for the electron transport in molecular junctions<sup>21,22,23,24</sup>, and the situation is still very much debated. Therefore, a more realistic and quantitative theoretical description of the surprisingly large effect is called for. The purpose of the present letter is to fill out this gap and study the influence of the junction environment on the the positions of the molecular levels in a realistic single-molecule SET. We have developed a scheme that includes the polarizable environment in a quantum chemical calculation, in which the static polarization response of the environment and the molecular charge distribution is determined self-consistently. Our calculations on the conjugated organic molecule used in experiments<sup>3,5</sup> show that a large part of the reduction of the addition energy can be accounted for by polarization of the environment. By using a simplified expression for the addition energy, the reduced addition energy can be understood in terms screening of the charging energy of the molecule and a

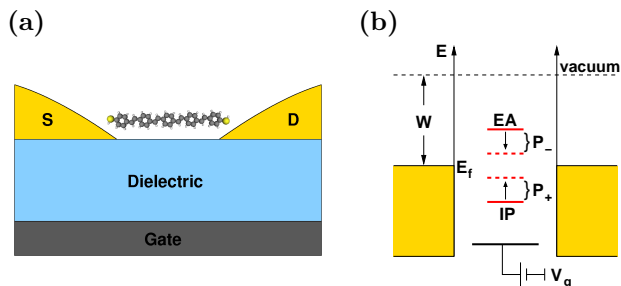


FIG. 1: (a) Schematic illustration of a three-terminal single-molecule transistor. (b) Energy level alignment in the molecular junction showing the position of the molecular ionization potential (IP) and electron affinity (EA) levels with respect to the work functions of the metallic leads. Also the gate electrode with voltage  $V_g$  which couples to EA and IP is schematically shown. The polarization shifts  $P_+$  and  $P_-$  of the levels due to the junction environment are indicated.

closing of the HOMO-LUMO gap.

For a single-molecule SET operating in the Coulomb blockade regime, i.e. with a weak tunnel coupling between the molecule and the source/drain electrodes, sequential tunneling is the dominating transport mechanism. In this regime charge transfer through the molecule is possible when either the IP or the EA is positioned within the bias window. If on the other hand no levels are present in the bias window, current is blocked and the molecule remain in a fixed charged state. To reach the regime where transport is possible one can either shift the IP and EA levels with the gate-voltage or apply a sufficiently large source-drain bias. This results in a so-called charge stability diagram which maps out the molecular charged states as a function of source-drain and gate voltage (see e.g. Figure 4). The addition energy  $U$  can be extracted from this diagram by measuring the height of the central diamond. Since the ionization potential and the electron affinity are given by the difference in total energy between the neutral molecule (with  $N$  electrons) and the cation ( $N - 1$ ) and anion ( $N + 1$ ), respectively,

$$\text{IP} = E^{N-1} - E^N \quad \text{and} \quad \text{EA} = E^N - E^{N+1} \quad (1)$$

the addition energy can be expressed as,

$$U = \text{IP} - \text{EA} = E^{N+1} + E^{N-1} - 2E^N. \quad (2)$$

When the molecule is placed in a nanojunction, charging of the molecule induces polarization charge in the junction environment. The formation of the polarization charge is associated with stabilizing polarization energies  $P_+$  (added hole) and  $P_-$  (added electron) for the cation and anion, respectively<sup>14</sup>, which shifts the IP and EA relative to their gas phase values as illustrated in Figure 1b. The resulting reduction of the addition energy is given by the sum  $P = P_+ + P_-$ , i.e.  $U = \text{IP}(g) - \text{EA}(g) - P$ . Naturally, the polarization energy  $P$  depends on the screening properties and response times of the environment. In single-molecule SETs where the typical current level is on the order of  $I \sim \text{pA} - \text{nA}$ , the polarization response of the metallic electrodes and gate dielectric (given by the plasmon frequency  $\sim 10^{15} \text{ s}^{-1}$  and the phonon frequency  $\sim 10^{13} \text{ s}^{-1}$  respectively) is orders of magnitudes faster than the tunneling rate  $\Gamma = I/e \sim 10^7 - 10^{10} \text{ s}^{-1}$  for electrons, implying that the polarization energy is given by the full static response of the environment.

In the Appendix we have provided a general framework for evaluating total energies of nanoscale systems in the presence of a polarizable environment. The main assumption of our approach is that the polarizable environment responds instantaneously to changes in the charge state of the molecule, which according to the above consideration is a reasonable assumption for single-molecule SETs. An electrostatic treatment of the environment hence suffices and we derive the following effective Hamiltonian for the nanojunction,

$$H = H_S + H_{pol} + H_{ext} \quad (3)$$

where  $H_S$  is the Hamiltonian of a general nanoscale system (in our case a molecule),

$$H_{pol} = \int d\mathbf{r} \rho_S(\mathbf{r})\Phi_{ind}(\mathbf{r}) - \frac{1}{2} \int d\mathbf{r} \langle \rho_S(\mathbf{r}) \rangle \Phi_{ind}(\mathbf{r}) \quad (4)$$

describes the interaction between the molecular charge distribution  $\rho_S$  and the polarization charge through the induced potential  $\Phi_{ind}$ , and

$$H_{ext} = \int d\mathbf{r} \rho_S(\mathbf{r})\Phi_{ext}(\mathbf{r}) \quad (5)$$

accounts for external voltages applied to the gate, source and drain electrodes. The external potential  $\Phi_{ext}$  satisfies Laplace equation with boundary-conditions given by the applied voltages on the electrodes. The induced potential  $\Phi_{ind}$  can be obtained via a solution to Poisson's equation

$$-\nabla \cdot [\varepsilon_r(\mathbf{r})\nabla\Phi(\mathbf{r})] = 4\pi\rho_S(\mathbf{r}), \quad (6)$$

for the potential  $\Phi = \Phi_S + \Phi_{ind}$ , where  $\varepsilon_r$  is the dielectric constant of the environment and  $\Phi_S$  the potential from the molecular charge distribution. The present approach thus allows for a continuum description of the environment combined with a quantum chemical treatment (e.g. DFT or Hartree-Fock) of the molecule. In order to account for the molecular charge redistribution due to the polarization response of the environment the induced potential must be included in the usual self-consistent cycle of e.g. DFT calculations.

In the present work a semi-empirical method has been combined with a finite element treatment of Poisson's equation (see Appendix A for details). We note that the addition energy we calculate for the isolated OPV5 molecule (see below), is underestimated with 1.2 eV as compared to the DFT value using the B3LYP exchange-correlation functional. In spite of this fact, we still expect the polarization energies to be accurate, since the interaction with the polarization charge is treated correctly in our approach. That this is indeed the case has been confirmed by comparison with other methods<sup>21</sup>.

We apply here our method to a single-molecule SETs based on the thiol-terminated OPV5 molecule, which is a organic conjugated molecule consisting of alternating phenylene and vinylene groups (see Figure 2b). In experimental realizations of OPV5-based SETs both heavily reduced addition energies, access to several redox states, molecular vibrational excitations and Kondo effect have been observed<sup>3,5,6</sup>. The simulated OPV5-SET is illustrated in Figure 2a with the molecule lying flat on the gate dielectric between the source and drain electrodes, which are separated by a 3.2 nm gap. The gate electrode is separated from the molecule by a 5 nm thick layer of gate oxide with dielectric constant  $\varepsilon_r = 10$ , corresponding to the high- $\kappa$  dielectric  $\text{Al}_2\text{O}_3$  often used in experiment. The relatively high dielectric constant of  $\text{Al}_2\text{O}_3$  ensures a reasonable capacitive coupling to the gate electrode. The gold electrodes are modelled by infinitely high metal blocks. The molecule is placed at a

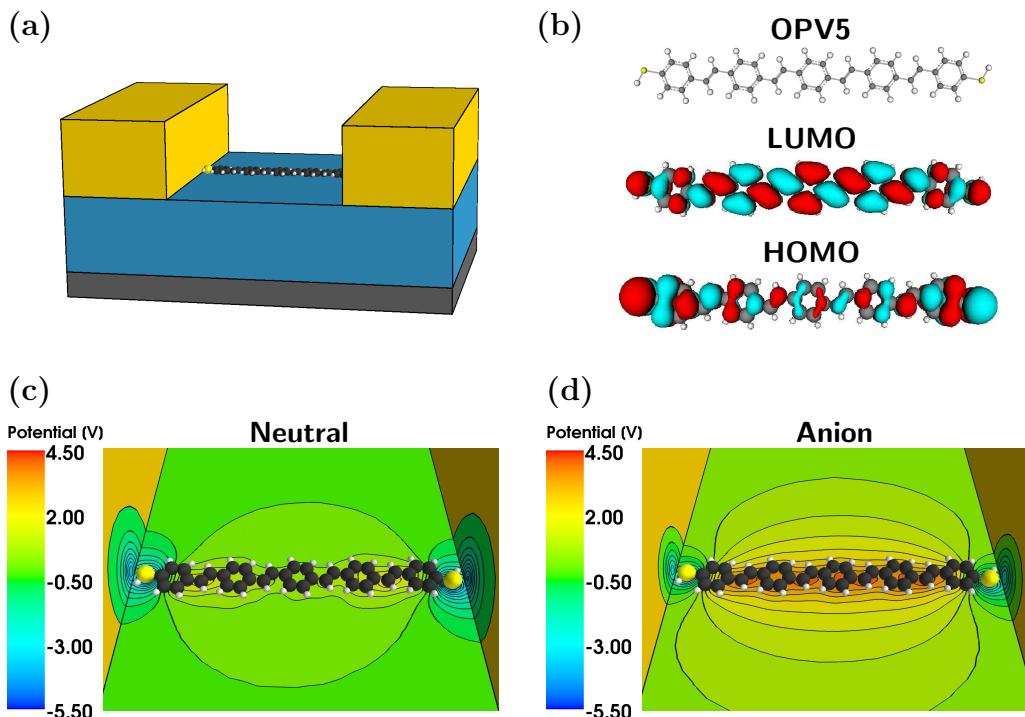


FIG. 2: (a) Illustration of the simulated OPV5-SET with the molecule lying flat on the Al<sub>2</sub>O<sub>3</sub> gate oxide between the source and drain electrodes. (b) Molecular structure of OPV5 and isosurface plots (blue: negative, red: positive) of the HOMO and LUMO orbitals for the isolated molecule. (c),(d) Polarization response of the nanojunction illustrated by contour plots of the induced potential from the polarization charge at the dielectric and electrode interfaces for the neutral molecule (c) and for the anion (d). Due to its partially positive charged thiol groups the overall neutral OPV5 molecule induces a negative potential in the nearby electrodes and dielectric that reduces the HOMO-LUMO gap (see text). The additional electron of the anion results in a significant polarization of the gate dielectric which reduces the charging energy of the molecule.

distance of 1 Å from the surfaces of the source/drain electrode and the gate oxide. Since the electrostatic image plane of atomic surfaces is located outside the atomic surface plane<sup>25,26</sup>, this effectively corresponds to a distance between the molecule and the surface atoms on the order of van der Waals distance ( $\sim 3$  Å).

Table I summarizes our findings for the addition energy, single-particle HOMO-LUMO gap and polarization energy in the following three environments: (i) gas phase, (ii) as in Figure 2a and (iii) molecule placed in the gap between two parallel metal surfaces separated by 3.2 nm. The polarization energies due to the presence of the junction environments results in significant reductions of the addition energies relative to their gas phase values.

For further analysis we shall use the following simplified interpretation of the addition energy: starting with two neutral molecules then  $U$  is the energy cost of transferring an electron from one molecule to other (see equation (2)). Since this process involves the promotion of an electron from the HOMO in one of the molecules to the LUMO in the other molecule, it is suggestive to write the addition energy as the HOMO-LUMO gap of the neutral molecule,  $\Delta_{HL}$ , plus two times the Coulomb energy,  $E_c$ , required to charge a molecule

$$U = \Delta_{HL} + 2E_c. \quad (7)$$

This is similar to the expression for the addition energy in the constant-interaction model, which has been used successfully for conventional quantum dot SETs<sup>27</sup>.

In a naive first guess one would expect the reduction of  $U$  to be mainly a consequence of screening of the charging energy  $E_c$ . However, Table I shows that also the HOMO-LUMO gaps are reduced in the polarizable environments. The origin of this reduction is illustrated in Figure 2c. Due to the positively charged thiol groups of the overall neutral OPV5, a negative electrostatic potential is induced in the nearby electrodes and dielectric. This combined with the localization of the HOMO on the thiol groups, see Figure 2b, shifts the HOMO level to higher energy. Similar reasoning for the negatively charged carbon backbone and the LUMO leads to a lowering of the LUMO level and hence a closing of the HOMO-LUMO gap. The charging energy obtained from equation (7) is for OPV5 in gas phase  $E_c = 1.08$  eV. The screening response of the nanojunction, which is shown for the OPV5 anion in Figure 2d, reduces this value to  $E_c = 75$  meV. We can therefore understand the reduction of the addition energy as a consequence of two parallel effects: i) a reduction of the HOMO-LUMO gap and ii) screening of the Coulomb repulsion on the molecule which lowers the charging energy. Since the majority of the reduction

environment	U	$\Delta_{HL}$	P
gas phase	3.27	1.12	-
SET	0.68	0.53	2.59
gap	2.08	0.92	1.19

TABLE I: Calculated addition energies,  $U$ , single-particle HOMO-LUMO gaps,  $\Delta_{HL}$ , and polarization energies,  $P$ , (all in eV) for the thiol-terminated OPV5-molecule in the three geometries: gas phase (isolated molecule), SET (geometry as in Figure 2a), and gap (molecule placed in the gap between two infinite parallel metal surfaces).

is due to the latter effect which is purely electrostatic in nature, the reduction for other molecules of the same size of OPV5 will be comparable. For smaller molecules we have found that the closer proximity of the polarization charge enhances the screening of the charging energy, resulting in a larger absolute reduction.

The important role of the gate oxide in the reduction of  $U$  is clearly demonstrated by the large difference in the polarization energy between the SET and gap environment in Table I. More than half of the polarization energy of 2.59 eV in the SET environment is due to the gate oxide. As the molecule is lying flat on the oxide which has almost metallic-like screening properties (the image charge strength of a dielectric surface is  $q_{\varepsilon_r} = \varepsilon_r/(\varepsilon_r + 1)$ ) this should come as no surprise. Note, however, that the polarization energy in the SET environment is highly dependent on the dielectric constant of the gate oxide. With a SiO<sub>2</sub> oxide layer ( $\varepsilon_r = 3.9$ ) the polarization energy is 2.11 eV. Due to its large distance to the molecule the gate electrode has no effect on the polarization energy.

As mentioned in the introductory part, the molecular levels can be probed by shifting them with the gate voltage or opening the source-drain bias window. Single-molecule SETs therefore provide a useful tool for measuring the energy differences between the molecular levels through the charge stability diagram, albeit in an unnatural environment. We have calculated the charge stability diagram for the OPV5 device by evaluating total energies of the neutral, singly charged and doubly charged molecule as a function of gate and source-drain voltage. The resulting stability diagram shown in Figure 4 is in qualitative agreement with experimental results<sup>3</sup>. It is characterized by two small diamonds enclosing a big central diamond. The height of the central diamond is seen to be  $\sim 0.50$  eV instead of 0.68 eV as we found for the zero bias value of the addition energy in Table I. This is due to the fact that the HOMO level moves downwards with the applied source-drain voltage, and hence decreasing the threshold for pulling out an electron from the HOMO. The non-linear edges on the left side of the central diamond is a result of this effect. The heights of the two smaller diamonds correspond to the addition energies of the anion and cation of the OPV5 molecule,

i.e.

$$U^{N\pm 1} = E^N + E^{N\pm 2} - 2E^{N\pm 1}. \quad (8)$$

The small addition energies associated with these states stem from their half filled frontier orbitals. Therefore, when adding/removing an electron to/from the anion/cation only the charging energy in equation (7) contributes. The resulting charging energies are  $\sim 50$  meV and  $\sim 85$  meV, respectively, showing that due to the different spatial distributions of the HOMO and LUMO, the charging energy of the cation and anion are not equal, which is implicitly assumed in equation (7)

One important ingredient in understanding the stability diagram is the gate coupling,  $\alpha = \partial E_{mol}/\partial V_g$ , i.e. how much the energy landscape on the molecule changes when a voltage is applied to the gate electrode. For usual quantum dot devices this is characterized by a single number, which assumes that all states couple equally to the gate. For the OPV5-SET considered here this is not the case. As shown in Figure 3a, the gate potential varies significantly over the extend of the molecule due to screening in the metallic electrodes, which results in a higher gate coupling to the LUMO compared to the HOMO. In the stability diagram this is reflected in the different slopes of the diamond edges, which are given by the gate couplings to the different charged states of the molecule. This has also been observed in a recent experiment<sup>6</sup>. The slopes of the diamond edges agree well with the calculated gate couplings in Figure 3b, where we read off the values  $\alpha_{\text{HOMO}} \sim 0.12$  and  $\alpha_{\text{LUMO}} \sim 0.25$  for an oxide thickness of 5 nm.

In conclusion, by using a method where a continuum description of the polarizable junction environment is combined with a quantum chemical calculation for the molecule, we have studied the effect of polarization in an OPV5 single-molecule SET. Our results show a significant modification of the addition energy caused by both a closing of the HOMO-LUMO gap and screening of the intra-molecular Coulomb interactions. Since the majority of the reduction is due to the latter effect, the reduction obtained here for OPV5, should be general for other molecules of same size. From the calculated charge stability diagram we explain at a qualitative level the origin of alternating diamond sizes, state dependent gate couplings and non-linear diamond edges, which all have been observed experimentally.

Our calculations explain a large part of the reductions observed experimentally, but certainly not all. Other effects not accounted for in the present work that can reduce the addition energy even further could be i) a geometry where the molecule is closer to the metallic electrodes as compared to our idealized setup ii) polaron formation upon charging of the molecule, i.e. relaxation of the nuclear configuration, which is associated with relaxation energies on the order of  $\sim 200 - 300$  meV<sup>28</sup> iii) a correlation induced localization of the added charge near the metallic electrodes beyond what can be captured by a mean-field approach.

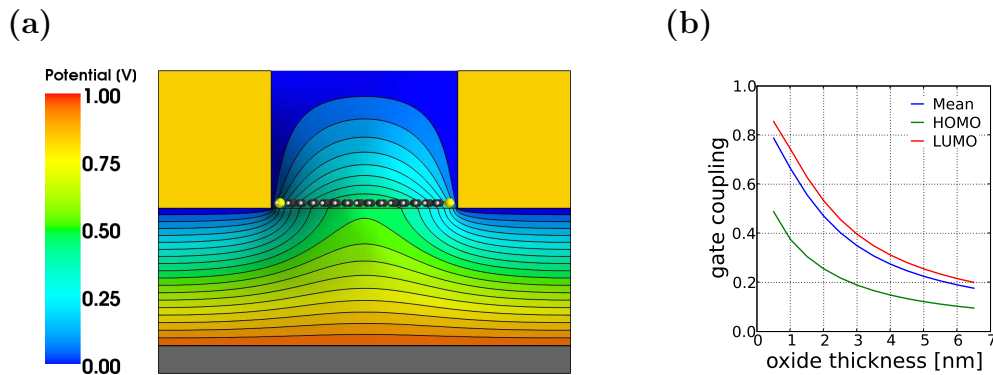


FIG. 3: (a) Contour plot of the gate potential for an oxide thickness of 2.5 nm and with 1 V applied to the gate electrode. The metallic electrodes, which are held at 0 V, screen the gate potential significantly which results in a stronger coupling to the central part of the molecule. (b) Gate couplings as a function of oxide thickness. The gate couplings have been calculated as follows: (Mean) by averaging the potential over the atomic positions of the molecule; (HOMO) and (LUMO) by calculating how much the levels move; both with 1 V applied to the gate electrode. The localization of the HOMO on the thiol groups results in a much lower gate coupling compared to the LUMO, which is delocalized over the carbon backbone of the molecule. For an oxide thickness of 5 nm the gate coupling (Mean) of  $\sim 0.2$  is in good agreement with the value reported in the experiment<sup>3</sup>.

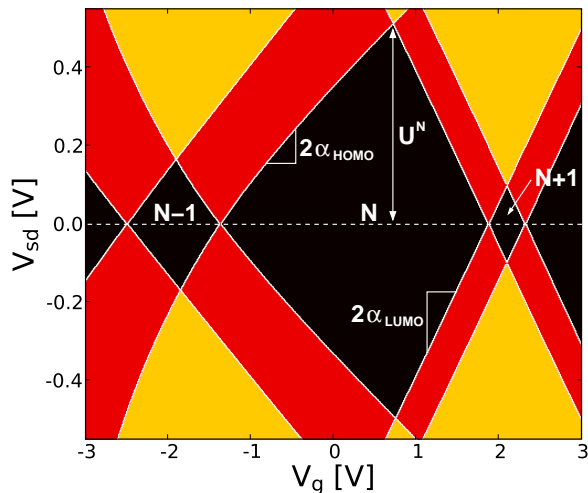


FIG. 4: Charge stability diagram for the OPV5-SET. The color indicates the number of levels positioned in the bias window (black: 0, red: 1, yellow: 2) and is hence an indirect measure of the current level for a given gate and source-drain voltage. The Fermi levels of the gold electrodes have been placed in the gap of the molecule as illustrated in Figure 1b. In each of the black diamonds current is blocked leaving the molecule in the indicated charge states. The addition energies of the charge states of the molecule can be read off from the heights of the respective diamonds.

**Acknowledgement.** We would like to thank T. Bjørnholm for illuminating discussions on the chemical aspects of the problem, K. Stokbro for useful inputs on the numerical calculations, Atomistix A/S for providing numerical routines for electronic structure calculations and people involved in the FEniCS project for providing useful insight in their FEM software. Financial support from the Danish Council for Production and Technology

(FTP) under grant 26-04-0181 ‘Atomic scale modeling of emerging electronic devices’ and the European Community’s Seventh Framework Programme (FP7/2007-2013) under grant ‘SINGLE’ no 213609 is acknowledged.

## APPENDIX A: SUPPORTING INFORMATION

### 1. Theoretical Framework

Here we show how to include the polarizable environment of a molecular single-electron transistor (SET) in a total energy calculation of the molecule. The main idea is the following: when treating the metallic leads and gate dielectric in a continuum description they enter only in the molecular Hamiltonian as an effective potential.

In order to address the position of the ionization potential and electron affinity in the molecular junction, the full junction Hamiltonian (i.e. molecule, metallic leads, gate dielectric and their mutual interaction) must be considered

$$H = H_S + H_E + H_{SE}. \quad (\text{A1})$$

The first term is the Hamiltonian of a nanoscale system  $S$  (here a molecule). In general,  $H_S$  is a quantum mechanical many-body Hamiltonian that can be treated with quantum chemical methods of required accuracy. For now  $H_S$  will not be specified further. The second term is the Hamiltonian of the polarizable environment ( $E$ ), which accounts for the energy cost due to build-up of the polarization charge in the metallic electrodes and the gate dielectric. Since the dynamical polarization response of the environment is orders of magnitude faster than the electronic tunneling rates between the molecule and leads, an electrostatic treatment of the interaction will be sufficient. Therefore we replace the environments

by their classical electrostatic energies, which are functionals of the charge distributions and polarizations in the leads and in the dielectric. This approximation neglects the kinetic energy and the exchange-correlation energy associated with the charge build up.

For the metallic environment where the electrons are free to move around the electrostatic energy is

$$H_m = \frac{1}{2} \int d\mathbf{r} \int d\mathbf{r}' \rho_m(\mathbf{r}) V_C(\mathbf{r} - \mathbf{r}') \rho_m(\mathbf{r}'), \quad (\text{A2})$$

where  $\rho_m$  is the charge density of the metal and  $V_C(\mathbf{r}) = 1/|\mathbf{r} - \mathbf{r}'|$  is the Coulomb interaction (atomic units are used throughout this note if not otherwise stated). In the dielectric environment the polarization charge is bound in small dipoles  $\mathbf{p}_i$ , giving rise to a macroscopic polarization  $\mathbf{P} = \sum_i \mathbf{p}_i$  of the dielectric. The energy of a polarized dielectric can be expressed as

$$H_d = \frac{1}{2} \int d\mathbf{r} \int d\mathbf{r}' \rho_b(\mathbf{r}) V_C(\mathbf{r} - \mathbf{r}') \rho_b(\mathbf{r}') + \frac{1}{2} \int d\mathbf{r} \frac{4\pi}{\chi(\mathbf{r}, \mathbf{r})} |\mathbf{P}(\mathbf{r})|^2, \quad (\text{A3})$$

where  $\rho_b = -\nabla \cdot \mathbf{P}$  is the bound charge of the dielectric and  $\chi$  the electric susceptibility. The first term in equation (A3) describes the electrostatic dipole-dipole interaction. The second local term, which is equivalent to the energy of a spring  $\frac{1}{2} kx^2$ , accounts for the energy stored in the dipoles  $\mathbf{p}_i$ . Utilizing that  $\nabla \cdot \frac{\mathbf{r} - \mathbf{r}'}{|\mathbf{r} - \mathbf{r}'|^3} = \delta(\mathbf{r} - \mathbf{r}')$  this term can recast in the form  $\frac{1}{2} \int d\mathbf{r} \int d\mathbf{r}' \rho_b(\mathbf{r}) \tilde{V}(\mathbf{r}; \mathbf{r}') \rho_b(\mathbf{r}')$ , where  $\tilde{V}$  is a complicated interaction between the bound charges. The total Hamiltonian of the environment can now be written

$$H_E = \frac{1}{2} \int d\mathbf{r} \int d\mathbf{r}' \rho_E(\mathbf{r}) V(\mathbf{r}; \mathbf{r}') \rho_E(\mathbf{r}'), \quad (\text{A4})$$

where  $\rho_E = \rho_m + \rho_d$  and  $V$  is either  $V_C$  or  $V_C + \tilde{V}$ . As we shall see in the following, a further specification of  $V$  is not required. The last term in equation (A1) accounts for the interaction between the molecule and the environment. Since we are focusing on the Coulomb blockade regime where the molecule has small tunnel couplings to the leads, the hybridization term of  $H_{SE}$  can be neglected. What remains is the Coulomb interaction between the spatially separated charges of the molecule and of the environment

$$H_{SE} = \int d\mathbf{r} \int d\mathbf{r}' \rho_S(\mathbf{r}) V_C(\mathbf{r} - \mathbf{r}') \rho_E(\mathbf{r}'). \quad (\text{A5})$$

Notice that the molecular charge has contributions from both the ionic cores and the valence electrons of the molecule:  $\rho_S(\mathbf{r}) = \rho_{ion}(\mathbf{r}) + \rho_e(\mathbf{r}) = \sum_i Z_i \delta(\mathbf{r} - \mathbf{r}_i) - \psi^\dagger(\mathbf{r}) \psi(\mathbf{r})$ .

With the Hamiltonian in place we now proceed to eliminate the environment degrees of freedom. Since the part of the Hamiltonian involving  $\rho_E$  is classical and has no

dynamics, the solution for  $\rho_E$  can be found by minimizing with respect  $\rho_E$ , i.e. by setting  $\delta H / \delta \rho_E = 0$ . The resulting equation can be solved for  $\rho_E$  giving (in matrix notation)

$$\rho_E = -[V_{EE}]^{-1} V_{ES} \rho_S \equiv \rho_{ind}, \quad (\text{A6})$$

which represents the charge density induced by the system charge  $\rho_S$ . Inserting this expression for the induced charge of the environment back into the full Hamiltonian in equation (A1), the terms involving  $\rho_E$  can be recast in the form

$$H_E + H_{SE} = -\frac{1}{2} \rho_S V_{SE} (V_{EE})^{-1} V_{ES} \rho_S, \quad (\text{A7})$$

in which the degrees of freedoms of the environment has been substituted by an effective interaction between molecular charges. By inserting the expression in equation (A6) for the induced charge density into equation (A7), we find that  $H_E + H_{SE} = \frac{1}{2} \rho_S V_{SE} \rho_{ind}$ , which is one half of  $H_{SE}$  in equation (A5). This result, which is a generalization of the classical image charge problem (a point charge placed at a distance  $z$  from a perfect conducting surface where  $H_E + H_{SE} = -1/4z$ ), states that the energy cost associated with the build up of the polarization charge is always one half of the energy gained by the system  $S$  through its interaction with the polarization charges.

Due to the presence of the electronic field operators in  $\rho_S$  the effective interaction in equation (A7) must be approximated. In our scheme we use a Hartree approximation. This is justified because i) correlation effects due to the effective interaction are small given the absence of a short range interaction and ii) exchange is not relevant since self-interactions are possible via the image charges. Introducing the induced potential  $\Phi_{ind}(\mathbf{r}) = \int d\mathbf{r}' \rho_{ind}(\mathbf{r}') / |\mathbf{r} - \mathbf{r}'|$ , the Hartree version of equation (A7) can be written as

$$H_E + H_{SE} = \int d\mathbf{r} \rho_S(\mathbf{r}) \Phi_{ind}(\mathbf{r}) - \frac{1}{2} \int d\mathbf{r} \langle \rho_S(\mathbf{r}) \rangle \Phi_{ind}(\mathbf{r}), \quad (\text{A8})$$

where the last term subtracts the double counted contributions to the total energy in the first term.

The induced potential can be obtained by solving Poisson's equation

$$-\nabla \cdot [\epsilon_r(\mathbf{r}) \nabla \Phi_{tot}(\mathbf{r})] = 4\pi \rho_S(\mathbf{r}) \quad (\text{A9})$$

with Dirichlet boundary-conditions on the electrode surfaces  $S_i$ , i.e.  $\Phi_{tot} = 0$  if  $\mathbf{r} \in S_i$ . Here, the total potential is the sum of the potential from the system charges plus the potential from the induced charges:  $\Phi_{tot} = \Phi_S + \Phi_{ind}$ .

The present approach thus allows us to combine a continuum description of the junction environment with a quantum chemical description of the molecule.

## 2. Semi-empirical Method

The molecular part of the total junction Hamiltonian in equation (A1) is split up into two parts: i) one that accounts for the isolated molecule and ii) one that accounts for polarization/redistribution of charge due to interactions with the junction environment and/or charging of the molecule,

$$H_s = H_0 + H_{pol}. \quad (\text{A10})$$

In the following our semi-empirical treatment is described in detail. It is similar to the one presented in Ref.<sup>29</sup>, however, here applied to total energy calculations and generalized to include dielectrics in the determination of the induced potential  $\Phi_{ind}$ .

The part describing the isolated molecule is an effective tight-binding Hamiltonian

$$H_0 = \sum_i \varepsilon_i c_i^\dagger c_i + \sum_{i \neq j} t_{ij} c_i^\dagger c_j, \quad (\text{A11})$$

where the sums run over atomic valence orbitals  $\{\phi_i\}$  and  $i$  is a collective index referring to atom, orbital and spin index:  $i \rightarrow \mu i \sigma$ . We use Extended Hückel parameters by Hoffmann<sup>30</sup> for the onsite and hopping energies

$$\varepsilon_i = -V_i \quad (\text{A12})$$

$$t_{ij} = \frac{1}{2} k S_{ij} (\varepsilon_i + \varepsilon_j). \quad (\text{A13})$$

Here  $V_i$  is associated with the ionization energy of the valence orbital  $\phi_i$ ,  $k$  is a fitting parameter usually set to 1.75 and  $S_{ij} = \langle \phi_i | \phi_j \rangle$  is the overlap between the non-orthogonal atomic orbitals. Notice that electron-electron interactions are implicitly included in  $H_0$  due to its parametrized form.

In the part of the Hamiltonian that accounts for polarization and charging of the molecule, electron-electron interactions are treated at the Hartree level. Since the Hartree potential of the isolated molecule is indirectly accounted for in  $H_0$ , only changes in the Hartree potential due to variations in the electron density from its value,  $n_0$ , in the isolated molecule are considered

$$\delta V_H(\mathbf{r}) = \int d\mathbf{r}' \frac{\delta n(\mathbf{r}')}{|\mathbf{r} - \mathbf{r}'|}, \quad (\text{A14})$$

where  $\delta n = n - n_0$ . Since the Hartree potential depends on the electron density, this poses a self-consistent problem that must be iterated to convergence.

To simplify the numerics the integral in equation (A14) is approximated by a sum over atomic point charges given by the Mulliken populations  $n_\mu = \text{Tr}[\rho S]_\mu$ , where  $\rho$  is the density matrix

$$\delta V_H(\mathbf{r}) = \sum_\mu \frac{\delta n_\mu}{|\mathbf{r} - \mathbf{r}_\mu|}. \quad (\text{A15})$$

To avoid problems with the diverging point charge potential when evaluated at the atomic positions,  $\mathbf{r}_\mu$ , the

onsite contribution to the sum is replaced by a species dependent Hubbard  $U$  taking into account the energy cost of adding an electron to the atom. These parameters are taken from the quantum chemical CNDO method<sup>31,32</sup>. In order to keep consistency between the onsite and the off-site interactions, the Magata-Nishimoto<sup>33</sup> interpolation formula is used for the latter

$$U_{\mu\nu} = \frac{1}{R_{\mu\nu} + \frac{2}{U_\mu + U_\nu}}. \quad (\text{A16})$$

With these approximation the final form of the Hartree potential in equation (A14) becomes

$$\delta V_H(\mathbf{r}_\mu) = \delta n_\mu U_\mu + \sum_{\nu \neq \mu} \delta n_\nu U_{\mu\nu}. \quad (\text{A17})$$

In our atomic basis the polarization/charging part of the Hamiltonian is written

$$H_{pol} = \sum_{i,j} V_{ij} c_i^\dagger c_j - \frac{1}{2} \sum_\mu n_\mu V_H(\mathbf{r}_\mu), \quad (\text{A18})$$

where the last term subtracts double counting in the first term and  $H_0$ . The matrix representation of the Hartree potential has been approximated as follows

$$V_i = \langle \phi_i | \delta V_H | \phi_i \rangle \approx \delta V_H(\mathbf{r}_\mu)$$

$$V_{ij} = \langle \phi_i | \delta V_H | \phi_j \rangle \approx \frac{1}{2} S_{ij} (V_i + V_j). \quad (\text{A19})$$

The part of the Hamiltonian involving the induced potential is written similarly

$$H_E + H_{ES} = \sum_{i,j} V_{ij} c_i^\dagger c_j - \frac{1}{2} \sum_\mu (Z_\mu - n_\mu) \Phi_{ind}(\mathbf{r}_\mu) \quad (\text{A20})$$

with  $V_{ij} = \langle \phi_i | V_{ind} | \phi_j \rangle$  evaluated as above in equation (A19).

## 3. Poisson's Equation and $\Phi_{ind}$

In the following section it is described how the induced potential is determined by solving Poisson's equation (A9) for the total potential  $\Phi_{tot}$ .

### a. Finite element approach

One of the major advantages of the finite element method (FEM) is its partitioning of the solution domain into a finite number of elements (typically triangles in 2D and tetrahedra in 3D). The possibility to refine the element size around sharp corners and in the vicinity of spatially rapidly varying source terms, allows FEM to handle a large variety of problems and solution domains of practically any geometry, hence making it very suitable for modelling of nanoscale devices.

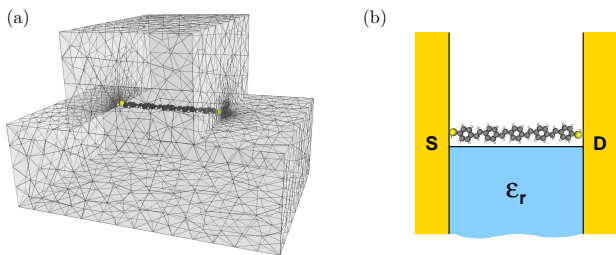


FIG. 5: **Finite element mesh and simplified junction geometry.** (a) Surface mesh for the OPV5-SET. (b) Simplified junction for which Poisson's equation can be solved analytically. In this geometry the electrodes are modelled by infinite metallic surfaces and the gate oxide as a semi-infinite dielectric layer sandwiched between the electrode surfaces. The gate electrode is not included (see text).

In the present case we seek to solve Poisson's equation in the geometry of a single-molecule SET. To this end we use the finite element software from the FEniCS project<sup>34</sup>.

The molecular charge density, which has both electronic and ionic contributions, is represented by a sum of atomic centered gaussian charge distributions:

$$\rho_s(\mathbf{r}) = (2\pi)^{-3/2} \sum_{\mu} \frac{q_{\mu}}{\sigma^3} e^{-|\mathbf{r}-\mathbf{r}_{\mu}|^2/2\sigma^2} \quad (\text{A21})$$

Here  $\sigma = a_0$  is the width of the gaussians and  $q_{\mu} = Z_{\mu} - n_{\mu}$  ( $Z_{\mu}$  being the atomic valence) is the net atomic charge.

Having obtained the total potential,  $\Phi_{tot}$ , the induced potential can be extracted by subtracting the potential,  $\Phi_s$ , from the molecular source charges, which for a gaussian charge distribution centered at the origin is:

$$\Phi_s(\mathbf{r}) = \frac{q}{r} \text{erf}\left(\frac{r}{\sqrt{2}\sigma}\right) \quad (\text{A22})$$

where erf is the error function.

The calculated induced potential has been converged (to 0.05 eV) with respect to the element size and the spatial dimensions of the device. In order to get an accurate description of the potential at the atomic positions, the molecule is enclosed in a box with a fine mesh of element size  $\sim a_0$ . The element size at the boundaries of the device are 20 times larger, which is illustrated by the boundary mesh in figure 5(a). The following device size was used to converge the potential: an electrode height of 50 a.u., a device width of 100 a.u. and a device length of 150 a.u..

#### b. Analytical solution

In the simplified device geometry shown in Fig. 5(b), Poisson's equation can be solved analytically. It can be shown that the Greens function satisfying:

$$-\nabla \cdot [\epsilon_r(\mathbf{r}) \nabla G(\mathbf{r}, \mathbf{r}')] = \delta(\mathbf{r} - \mathbf{r}') \quad (\text{A23})$$

has the following image charge solution:

$$G(\mathbf{r}, \mathbf{r}') = \sum_{\sigma=\pm 1} \sum_{\tau=\pm 1} \sigma \left( \frac{\epsilon_r + \tau}{\epsilon_r + 1} \right) \tau \left[ \frac{1}{\sqrt{(x - \sigma x')^2 + (y - \tau y')^2 + (z - z')^2}} + \sum_{n=1}^{\infty} \left( \frac{1}{\sqrt{(2nL - (x - \sigma x'))^2 + (y - \tau y')^2 + (z - z')^2}} + \frac{1}{\sqrt{(2nL + (x - \sigma x'))^2 + (y - \tau y')^2 + (z - z')^2}} \right) \right] \quad (\text{A24})$$

where  $L$  is the electrode spacing ( $z$  is the direction perpendicular to the paper plane in Fig. 5(b)) and the sums run over all repeated images of the source charge in the metallic surfaces and the dielectric. By leaving out the contribution from the source charge itself, only the induced potential remains:

$$\Phi_{ind}(\mathbf{r}) = \tilde{G}(\mathbf{r}, \mathbf{r}') \quad (\text{A25})$$

Here  $\tilde{G}$  denotes the Greens function which does not include the  $\sigma = 1$  and  $\tau = 1$  term outside the  $n$ -sum in equation (A24).

In the calculations using the analytical solution, the molecular charge distribution has been approximated by point charges  $q_{\mu}$  located at the atomic positions. The induced potential follows directly from the Greens functions of the individual point charges:

$$\Phi_{ind}(\mathbf{r}) = \sum_{\mu} q_{\mu} \tilde{G}(\mathbf{r}, \mathbf{r}_{\mu}) \quad (\text{A26})$$



Molecule	FEM	Analytic
OPV2	3.56	3.63
OPV3	3.11	3.17
OPV4	2.81	2.87
OPV5	2.59	2.63

TABLE II: Calculated polarization energies  $P$  (in eV) for the two junction geometries illustrated in figure 5. The same electrode spacing has been used in the two geometries. Due to the infinite metallic surfaces, the polarization energy is slightly larger for the simplified junction geometry.

### c. FEM vs analytic

Table II summarizes the calculated polarization energies for the realistic junction modelled with FEM and the

simplified junction shown in Fig. 5(b). The difference between the polarization energies in the two junctions is on the order of  $\sim 50$  meV for the different OPV-molecules. The slightly larger polarization energies in the simplified junction stem from the infinite metallic electrodes, which screen the Coulomb interactions on the molecule better than the semi-infinite metal blocks of the realistic junction. Notice that, due to its large distance to the molecule ( $\sim 5$  nm) and the metallic-like screening properties of the  $\text{Al}_2\text{O}_3$  gate oxide, the gate electrode does not contribute to the polarization energy in the realistic junction. This explains the relative small differences between the polarization energies in the two junction geometries.

Hence, our analytical solution provides a realistic description of the potential in generic SET geometry (Fig. 2(a) in the main part of the paper) that can be used instead of computationally heavy Poisson solvers.

- 
- <sup>1</sup> Liang, W.; Shores, M. P.; Bockrath, M.; Long, J. R.; Park, H. *Nature* **2002**, *417*, 725.
- <sup>2</sup> Park, J.; Pasupathy, A. N.; Goldsmith, J. I.; Chang, C.; Yaish, Y.; Petta, J. R.; Rinkoski, M.; Sethna, J. P.; Abruña, H. D.; McEuen, P. L.; Ralph, D. C. *Nature* **2002**, *417*, 722.
- <sup>3</sup> Kubatkin, S.; Danilov, A.; Hjort, M.; Cornil, J.; Brédas, J.-L.; S.-Hansen, N.; Hedegård, P.; Bjørnholm, T. *Nature* **2003**, *425*, 698.
- <sup>4</sup> Yu, L. H.; Keane, Z. K.; Ciszek, J. W.; Cheng, L.; Tour, J. M.; Baruah, T.; Pederson, M. R.; Natelson, D. *Phys. Rev. Lett.* **2005**, *95*, 256803.
- <sup>5</sup> Osorio, E. A.; O'Neill, K.; Stuhr-Hansen, N.; Nielsen, O. F.; Bjørnholm, T.; van der Zant, H. S. J. *Adv. Mater.* **2007**, *19*, 281.
- <sup>6</sup> Osorio, E. A.; O'Neill, K.; Wegewijs, M.; Stuhr-Hansen, N.; Paaske, J.; Bjørnholm, T.; van der Zant, H. S. J. *Nano. Lett.* **2007**, *7*, 3336.
- <sup>7</sup> Chae, D.-H.; Berry, J. F.; Jung, S.; Cotton, F. A.; Murillo, C. A.; Yao, Z. *Nano. Lett.* **2006**, *6*, 165.
- <sup>8</sup> Danilov, A.; Kubatkin, S.; Kafanov, S.; Hedegård, P.; Stuhr-Hansen, N.; Moth-Poulsen, K.; Bjørnholm, T. *Nano. Lett.* **2008**, *8*, 1.
- <sup>9</sup> Ahn, C. H.; Bhattacharya, A.; Ventra, M. D.; Eckstein, J. N.; Frisbie, C. D.; Gershenson, M. E.; Goldman, A. M.; Inoue, I. H.; Mannhart, J.; Millis, A. J.; Morpurgo, A. F.; Natelson, D.; Triscone, J.-M. *Rev. Mod. Phys.* **2006**, *78*, 1185.
- <sup>10</sup> Thijssen, J. M.; van der Zant, H. S. J. *phys. stat. sol. (b)* **2008**.
- <sup>11</sup> Inkson, J. C. *J. Phys. C* **1973**, *6*, 1350.
- <sup>12</sup> Charlesworth, J. P. A.; Godby, R. W.; Needs, R. J. *Phys. Rev. Lett.* **1993**, *70*, 1685.
- <sup>13</sup> Hesper, R.; Tjeng, L. H.; Sawatzky, G. A. *Europhys. Lett.* **1997**, *40*, 177.
- <sup>14</sup> Tsiper, E. V.; Soos, Z. G.; Gao, W.; Kahn, A. *Chem. Phys. Lett.* **2002**, *360*, 47.
- <sup>15</sup> Veenstra, S. C.; Jonkman, H. T. *J. Polym. Sci. B: Polym. Phys.* **2003**, *41*, 2549.
- <sup>16</sup> Zhu, X.-Y. *J. Phys. Chem. B* **2004**, *108*, 8778.
- <sup>17</sup> Lu, X.; Grobis, M.; Khoo, K. H.; Louie, S. G.; Crommie, M. F. *Phys. Rev. B* **2004**, *70*, 115418.
- <sup>18</sup> Repp, J.; Meyer, G.; Stojković, S. M.; Gourdon, A.; Joachim, C. *Phys. Rev. Lett.* **2005**, *94*, 026803.
- <sup>19</sup> Marcus, R. A. *J. Chem. Phys.* **1965**, *43*, 679.
- <sup>20</sup> Hedegård, P.; Bjørnholm, T. *Chemical Physics* **2005**, *319*, 350.
- <sup>21</sup> Neaton, J. B.; Hybertsen, M. S.; Louie, S. G. *Phys. Rev. Lett.* **2006**, *97*, 216405.
- <sup>22</sup> Yeganeh, S.; Galperin, M.; Ratner, M. A. *J. Am. Chem. Soc.* **2007**, *129*, 13313.
- <sup>23</sup> Quek, S. Y.; Venkataraman, L.; Choi, H. J.; Louie, S. G.; Hybertsen, M. S.; Neaton, J. B. *Nano. Lett.* **2007**, *7*, 3477.
- <sup>24</sup> Mowbray, D. J.; Jones, G.; Thygesen, K. S. *J. Chem. Phys.* **2008**, *128*, 111103.
- <sup>25</sup> Lam, S. C.; Needs, R. J. *J. Phys.: Condens. Matter* **1993**, *5*, 2101.
- <sup>26</sup> Chulkov, E. V.; Silkin, V. M.; Echenique, P. M. *Surf. Sci.* **1999**, *437*, 330.
- <sup>27</sup> Kouwenhoven, L. P.; Austing, D. G.; Tarucha, S. *Rep. Prog. Phys.* **2001**, *64*, 701.
- <sup>28</sup> Geskin, V. M.; Cornil, J.; Brédas, J. L. *Chem. Phys. Lett.* **2005**, *403*, 228.
- <sup>29</sup> Zahid, F.; Paulsson, M.; Polizzi, E.; Ghosh, A. W.; Siddiqui, L.; Datta, S. *J. Chem. Phys.* **2005**, *123*, 064707.
- <sup>30</sup> Hoffmann, R. *J. Chem. Phys.* **1963**, *39*, 1397.
- <sup>31</sup> Fulde, P. *Electron Correlations in Molecules and Solids*, 3rd ed.; Springer Series in Solid-State Sciences 100; Springer: Berlin, 1995.
- <sup>32</sup> Pople, J. A.; Segal, G. A. *J. Chem. Phys.* **1966**, *44*, 3289.
- <sup>33</sup> Sichel, J. M.; Whitehead, M. A. *Theor. Chem. Acc.* **1968**, *11*, 220.
- <sup>34</sup> FEniCS Project, <http://www.fenics.org/>.